

Thermally driven quantum refrigerator autonomously resets superconducting qubit

Mohammed Ali Aamir,^{1,*} Paul Jamet Suria,¹ José Antonio Marín Guzmán,² Claudia Castillo-Moreno,¹ Jeffrey M. Epstein,^{2,3} Nicole Yunger Halpern,^{2,3,†} and Simone Gasparinetti^{1,‡}

¹*Department of Microtechnology and Nanoscience,
Chalmers University of Technology, 412 96 Gothenburg, Sweden*

²*Joint Center for Quantum Information and Computer Science,
NIST and University of Maryland, College Park, MD 20742, USA*

³*Institute for Physical Science and Technology, University of Maryland, College Park, MD 20742, USA*
(Dated: May 29, 2023)

The first thermal machines steered the industrial revolution, but their quantum analogs have yet to prove useful. Here, we demonstrate a useful quantum absorption refrigerator formed from superconducting circuits. We use it to reset a transmon qubit to a temperature lower than that achievable with any one available bath. The process is driven by a thermal gradient and is autonomous—requires no external control. The refrigerator exploits an engineered three-body interaction between the target qubit and two auxiliary qubits coupled to thermal environments. The environments consist of microwave waveguides populated with synthesized thermal photons. The target qubit, if initially fully excited, reaches a steady-state excited-level population of $5 \times 10^{-4} \pm 5 \times 10^{-4}$ (an effective temperature of 23.5 mK) in about 1.6 μ s. Our results epitomize how quantum thermal machines can be leveraged for quantum information-processing tasks. They also initiate a path toward experimental studies of quantum thermodynamics with superconducting circuits coupled to propagating thermal microwave fields.

Quantum thermodynamics should be more useful. The field has yielded fundamental insights, such as extensions of the second law of thermodynamics to small, coherent, and far-from-equilibrium systems [1–13]. Additionally, quantum phenomena have been shown to enhance engines [14–19], batteries [20], and refrigeration [21, 22]. These results are progressing gradually from theory to proof-of-principle experiments. However, quantum thermal technologies remain experimental curiosities, not practical everyday tools. Key challenges include control [23] and cooling quantum thermal machines to temperatures that support quantum phenomena. Both challenges require substantial energy and effort but yield small returns. For example, one would expect a single-atom engine to perform only about an electronvolt of work [24].

Autonomous quantum machines offer hope. First, they operate without external control. Second, they run on heat drawn from thermal baths, which are naturally abundant [25]. A quantum thermal machine would be useful in a context that met three criteria: (i) The machine fulfills a need. (ii) The machine can access natural different-temperature baths. (iii) Maintaining the machine’s coherence costs no extra expense.

We identify such a context: qubit reset. Consider a superconducting quantum computer starting a calculation. The computer requires qubits initialized to their ground states. If left to thermalize with its environment as thoroughly as possible, though, the qubit could achieve only an excited-state population of ≈ 0.01 to 0.03, or an effective

temperature of 45 mK to 70 mK [26–29]. Furthermore, such passive thermalization takes a few multiples of the qubit’s energy-relaxation time—hundreds of microseconds in state-of-the-art setups—delaying the next computation. A quantum machine cooling the qubits to their ground (minimal-entropy) states fulfills criterion (i). Moreover, superconducting qubits inhabit a dilution refrigerator formed from nested plates, whose temperatures decrease from the outermost plate to the innermost. These temperature plates can serve as heat baths, meeting criterion (ii). Finally, the machine can retain its quantum nature if mounted on the coldest plate, next to the quantum processing unit, satisfying criterion (iii). Such an autonomous machine would be a *quantum absorption refrigerator*.

Quantum absorption refrigerators have been widely studied theoretically [30–49]. Reference [50] reported a landmark proof-of-principle experiment performed with trapped ions. However, the heat baths were emulated with electric fields and lasers, rather than natural sources. Other quantum refrigerators, motivated by possible applications, have been proposed [51, 52] and tested [53–55] but are not autonomous.

We report on a quantum absorption refrigerator realized with superconducting circuits. Our quantum refrigerator cools and therefore resets a target superconducting qubit *autonomously*. The target qubit’s energy-relaxation time is fully determined by the temperature of a hot bath we can vary. Using this control, we can vary the energy-relaxation time by a factor of > 60 . The reset’s fidelity is competitive: The target’s excited-state population reaches as low as 5×10^{-4} (effective temperatures as low as 23.5 mK). In comparison, state-of-the-art reset protocols achieve populations of 8×10^{-4} to 2×10^{-3} (effective temperatures of 40 mK to 49 mK) [28, 29].

* aamir.ali@chalmers.se

† nicoleyh@umd.edu

‡ simoneg@chalmers.se

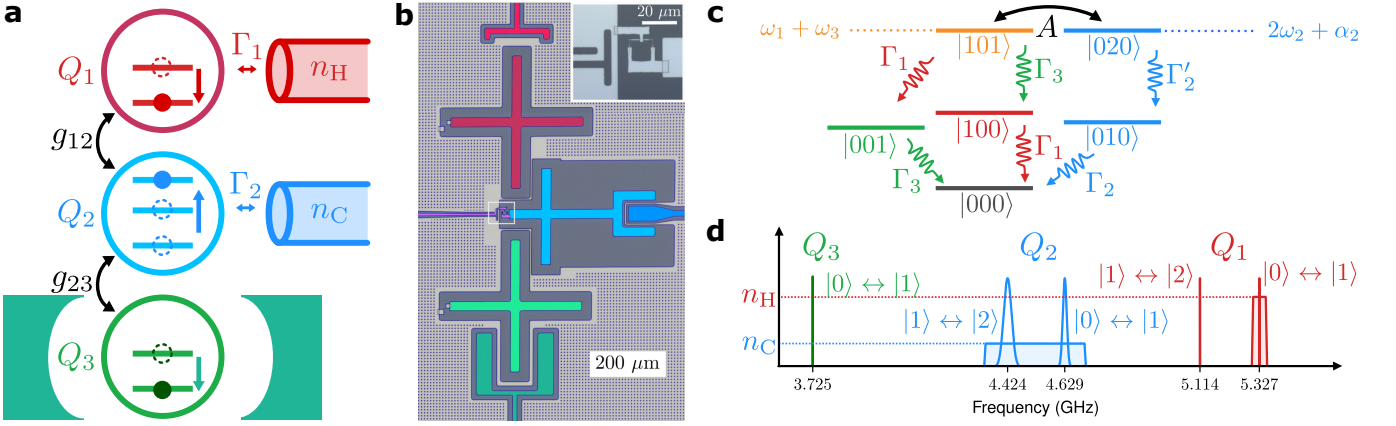


FIG. 1: Absorption-refrigerator scheme and level diagram. (a) Scheme of quantum absorption refrigerator with three qudits. Qubit Q_1 couples directly to a waveguide at the rate Γ_1 ; and qudit Q_2 , to another waveguide at the rate Γ_2 . The waveguides, operating as thermal baths, host thermal photons of average numbers n_H and n_C . A single excitation in Q_1 and a single excitation in Q_3 are simultaneously exchanged with a double excitation in Q_2 . This exchange, occurring under a resonance condition, helps reset Q_3 . (b) False-color micrograph of the device implemented with superconducting circuits. Q_2 is frequency-tunable, due to a flux current line and two parallel Josephson junctions, magnified in the inset. (c) Level diagram showing tensor products $|q_1 q_2 q_3\rangle$ of the qudits' respective energy eigenstates. $|101\rangle$ and $|020\rangle$ are resonant if $\omega_1 + \omega_3 = 2\omega_2 + \alpha_2$. At resonance, a three-body interaction couples the states at a rate A . (d) Distributions over the qudits' experimentally observed transition frequencies. The Lorentzian distributions' widths represent spectral widths. The red shaded box depicts the spectral density n_H of photons injected into the waveguide coupled to Q_1 . This synthesized noise realizes the refrigerator's hot thermal bath. Analogous statements concern the blue box, n_C , Q_2 , and the cold bath.

Our experiment demonstrates that quantum thermal machines not only can be useful, but also can be integrated with quantum information-processing units. Furthermore, such a practical autonomous quantum machine costs less control and thermodynamic work than its nonautonomous counterparts [56–58].

Our absorption refrigerator consists of three qudits (d -level quantum systems), as depicted in Fig. 1a. The auxiliary qudits Q_1 and Q_2 correspond to $d = 2, 3$, respectively. The qubit Q_3 is the target of the refrigerator's cooling. Nearest-neighbor qudits couple together with strengths g_{12} and g_{23} . These couplings can lead to an effective three-body interaction [59], a crucial ingredient in a quantum absorption refrigerator [25, 30, 31, 36]. We engineer the three-body interaction such that one excitation in Q_1 and one in Q_3 are simultaneously, coherently exchanged with a double excitation in Q_2 . Each of Q_1 and Q_2 couples directly to a waveguide that can serve as a heat bath. Each waveguide, supporting a continuum of electromagnetic modes, can be populated with thermal photons of average number n_H or n_C .

The qudits are Al-based superconducting transmons that have Al/AlO_x/Al Josephson junctions [60]. We arrange the qudits spatially in a linear configuration (Fig. 1b). The capacitances between the transmons couple them mutually. Qudit Q_1 has a transition frequency $\omega_1/(2\pi) = 5.327$ MHz; and qudit Q_2 , a variable frequency $\omega_2/(2\pi)$. Q_1 couples capacitively to a microwave waveguide directly, at a dissipation rate $\Gamma_1/(2\pi) = 70$ kHz; and Q_2 couples to another waveguide at $\Gamma_2/(2\pi) = 7.2$ MHz. The third qubit, Q_3 , has a transition frequency $\omega_3/(2\pi) = 3.725$ GHz. Q_3 couples

dispersively to a coplanar waveguide resonator. Via the resonator, we read out Q_3 's state and drive Q_3 coherently. In our proof-of-concept demonstration, Q_3 stands in for a computational qubit that is being reset and that may participate in a larger processing unit. In the present design, Q_3 has a natural energy-relaxation time $T_{\text{relax}} = 16.8$ μs , limited largely by Purcell decay into the nearest waveguide, and a residual excited-state population $P_0 = 0.028$. In future realizations, one can increase T_{relax} using Purcell filters [61].

The interqudit couplings hybridize the qudit modes. The hybridization, together with the Josephson junctions' nonlinearity, results in a three-body interaction (see SI). For this interaction to be resonant, the qudit frequencies must meet the condition $\omega_1 + \omega_3 = 2\omega_2^{\text{res}} + \alpha_2$. The ω_2^{res} denotes the Q_2 frequency that satisfies the equality, and α_2 denotes Q_2 's anharmonicity. The interaction arises from a four-wave mixing process: One excitation in Q_1 and one excitation in Q_3 are simultaneously exchanged with a double excitation in Q_2 (Fig. 1a) [59]. To control the resonance condition *in situ*, we make Q_2 frequency-tunable [60]. We control the frequency with a magnetic flux induced by a nearby current line. The device is mounted in a dilution refrigerator that reaches 10 mK.

To detail the resonance condition, we introduce further notation. Denote by $|0\rangle$ and $|1\rangle$ any qudit's ground and first-excited states. Denote by $|2\rangle$ Q_2 's second excited state. We represent a three-qudit state by $|q_1 q_2 q_3\rangle := |q_1\rangle_1 \otimes |q_2\rangle_2 \otimes |q_3\rangle_3$. The resonance condition implies that $|101\rangle$ and $|020\rangle$ are resonant (Fig. 1c). Two processes, operating in conjunction, reset Q_3 : (i) Levels $|101\rangle$ and

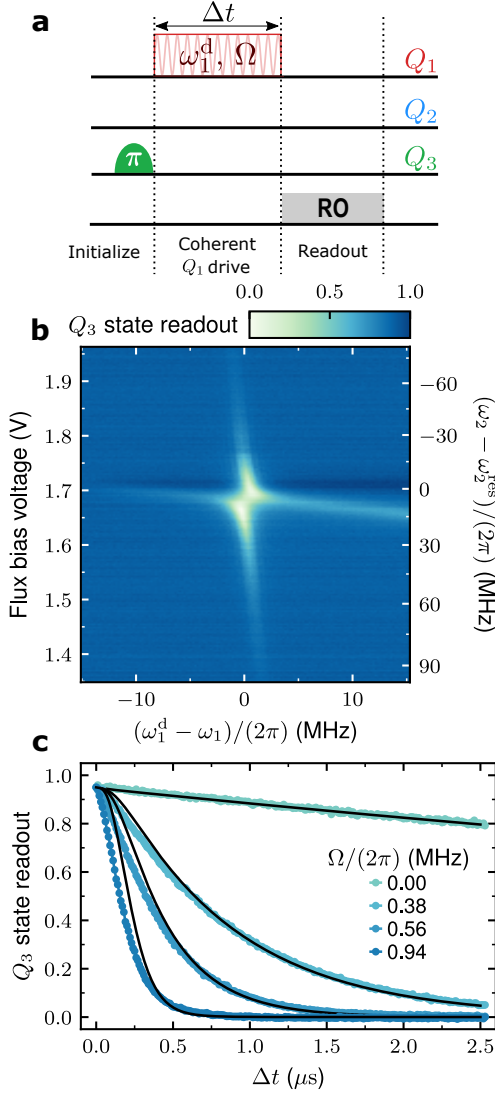


FIG. 2: Three-body interaction: (a) Pulse scheme. See text for description. (b) 2D plot of Q_3 's excited-state population ($[(\sigma_z) + \mathbb{1}]/2$), as a function of (i) the flux current (left axis) modulating Q_2 's frequency and (ii) the detuning between the Q_1 -drive frequency $\omega_1^d/(2\pi)$ and $\omega_1/(2\pi)$ (bottom axis). Q_1 is driven for $\Delta t = 2 \mu\text{s}$ during the pulse scheme, after which we read out (RO) Q_3 's state via the resonator. The left axis translates directly into the right axis—the detuning of the Q_2 frequency, $\omega_2/(2\pi)$, from the resonant value, $\omega_2^{\text{res}}/(2\pi)$. The white patch evidences an avoided crossing, where $|101\rangle$ and $|020\rangle$ become resonant (Fig. 1c). (c) Q_3 's excited-state readout, as a function of the duration Δt of the Q_1 drive, at select drive rates $\Omega/(2\pi)$. Solid black lines are fits based on model the in Sec. II of the SI.

$|020\rangle$ coherently couple with an effective strength A . (ii) Q_2 dissipates into its waveguide at the rate Γ_2 . The combined action of (i) and (ii) brings $|101\rangle$ rapidly to $|010\rangle$ (and then to $|000\rangle$), thereby resetting Q_3 .

We raise the temperature of each heat bath (realized with a waveguide) as follows. We inject radiation with

a thermal spectral profile over a frequency range that covers the relevant qubits' energy-level transitions. The radiation impinging on the qubits results from admixing quantum vacuum fluctuations from a cold (10 mK) resistor and classical microwave noise synthesized at room temperature [62, 63]. We admix the ingredients using a dissipative microwave attenuator (a resistor network) functioning as a beam splitter for microwave fields. The synthesized noise has a finite bandwidth larger than Q_1 's and Q_2 's spectral widths. The noise spans a frequency range that covers Q_1 's transitions ($|0\rangle \leftrightarrow |1\rangle$) and Q_2 's transitions ($|0\rangle \leftrightarrow |1\rangle$ and $|1\rangle \leftrightarrow |2\rangle$) (Fig. 1d). This setup enables the whole system to function as a quantum thermal machine. The thermal baths induce transitions in Q_1 and Q_2 , autonomously driving the reset by virtue of the three-body interaction.

Having specified the setup, we demonstrate the three-body interaction: We verify that Q_3 can be reset via resonantly driving of Q_1 if and only if Q_2 meets the resonance condition. The qubits begin in $|000\rangle$, whereupon we issue two microwave drive pulses (Fig. 2a). The first is a Gaussian π -pulse that excites Q_3 to state $|1\rangle$: $|000\rangle \rightarrow |001\rangle$. The second pulse is flat and coherently drives Q_1 (effecting $|001\rangle \leftrightarrow |101\rangle$) at the frequency ω_1^d with a rate Ω , for a duration Δt . Subsequently, we perform qubit-state readout on Q_3 (we measure $[(\sigma_z) + \mathbb{1}]/2$) via Q_3 's resonator. We investigate the readout's dependences on ω_1^d and on the flux current that modulates the tunable Q_2 frequency. We have fixed $\Delta t = 2 \mu\text{s}$ and $\Omega/(2\pi) = 200 \text{ kHz}$. The microwave drives, we observe, deplete Q_3 's excited-state population (Fig. 2a). The depletion is greatest when $\omega_2 = \omega_2^{\text{res}}$ and the drive is resonant ($\omega_1^d = \omega_1$)—when the resonant coupling A between $|101\rangle$ and $|020\rangle$ is strongest.

Q_3 's excited state is depleted by the cascaded processes $|001\rangle \leftrightarrow |101\rangle \leftrightarrow |020\rangle \rightarrow |010\rangle$. Away from the resonance condition, the resonant coupling A decreases. Consequently, Q_3 's excited-state population drops less as the $|101\rangle$ – $|020\rangle$ detuning grows. Furthermore, we study the effect of increasing Ω (Fig. 2c). When $\Omega = 0 \text{ MHz}$, Q_3 decays to its ground state (resets) at its natural energy-relaxation time, T_{relax} . As Ω increases, the reset happens increasingly quickly. According to our model's fit to these results, the 3-body interaction strength is $A/(2\pi) = 3.2 \text{ MHz}$.

Having demonstrated the three-body interaction, we operate the three-qubit system as a quantum thermal machine. To measure the system's performance, we implement a three-step pulse sequence (Fig. 3a): (i) Excite Q_3 to near $|1\rangle$ (to an excited-state population of 0.95). (ii) Fill the waveguides with the thermal photons, as described above, for a variable time interval Δt . (iii) Measure Q_3 's excited-state population, using a Rabi population-measurement scheme [26, 27] (see Sec. III of the Supplementary Information [SI] for details). This scheme allows for a more accurate population measurement than does standard qubit-state readout.

We raise the hot bath's effective temperature and in-

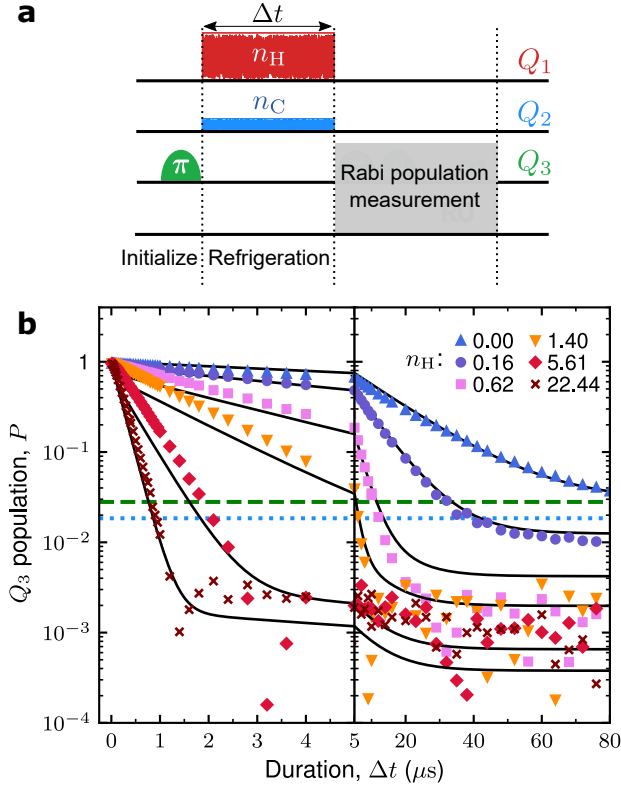


FIG. 3: Autonomous refrigeration enabled by hot thermal bath. (a) 3-step pulse scheme: Initialization brings Q_3 's excited-state population close to $|1\rangle$. During refrigeration, Q_1 and Q_2 interact with synthesized thermal fields for a duration Δt . Finally, the Q_3 population, P , is measured via a Rabi population-measurement scheme (see SI). (b) Q_3 population as a function of the time Δt , at select values of n_H , the average number of photons in the hot bath. Q_2 experiences no synthesized thermal field; due to the residual thermal field, $n_C \approx 0.007$, we estimate. The dashed green line shows Q_3 's residual excited-state population (defined in the main text), 0.028. The dotted blue line shows the excited-state population that Q_3 would have at the cold bath's temperature (45 mK), 0.020. The uncertainty in our P measurement, 0.0005, quantifies the noise floor. As P approaches 0.0005, therefore, the measured data appear to exhibit a greater dispersion. All solid lines are fits based on the model in Sec. II of the SI.

investigate how Q_3 's excited-state population, P , responds. To do so, we elevate the average number n_H of thermal photons in the hot bath, by increasing the spectral power of the synthesized noise in Q_1 's waveguide. We perform this study in the absence of synthesized noise in the cold bath (coupled to Q_2). In independent measurements, we determine the cold bath's average number of thermal photons: $n_C = 0.007$, associated with a temperature $T_C = 45$ mK. The greater the n_H , the more quickly P decays as we increase Δt (Fig. 3b). At the low value $n_H = 0.16$, P drops below the residual excited-state population P_0 (green dashed line in Fig. 3b), which Q_3 would achieve if left alone for a long time. The resid-

ual population corresponds to an effective temperature of $T_T = 50$ mK. If thermalized at the cold bath's temperature (45 mK), Q_3 would have an excited-state population $P_0 = 0.020$ (blue dotted line). Notably, if the hot bath is excited, Q_3 reaches a steady-state population P_{SS} an order of magnitude lower than P_0 and P_C . Our refrigeration scheme clearly outperforms passive thermalization with either Q_3 's intrinsic bath or the coldest bath available.

At $n_H = 21.424$ ($T_H = 5.6$ K), the refrigeration reduces Q_3 's effective energy-relaxation time, T_{relax} , from $16.8 \mu s$ to 250 ns, a reduction by a factor of over 60. Q_3 's population declines to 2×10^{-3} over $1.6 \mu s$, before asymptotically approaching a steady state. We define Q_3 's steady-state population as $P_{SS} := P(\Delta t = 100 \mu s)$. P_{SS} reaches a minimum of $5 \times 10^{-4} \pm 5 \times 10^{-4}$, equivalent to a temperature of 23.5 mK.

A refrigerator's thermodynamic figure of merit is its coefficient of performance (COP) [36]. The COP equals the heat current expelled by the target, divided by the heat current drawn by Q_1 from the hot bath. We calculate the steady-state COP numerically from the theoretical model in Sec. II of the SI. The steady-state COP is 0.7 when $T_H = 5.6$ K and $T_T = 23.5$ mK. The Carnot bound on our COP is $\frac{T_T(T_H - T_C)}{T_H(T_C - T_T)} = 1.1 > 0.7$. For comparison, a common autonomous air conditioner has a COP of ≈ 0.7 [64].

Another important performance metric is the time required to reset Q_3 . We define the reset time as the time required for P to reach 0.01 (corresponding to 38.5 mK). The reset time reaches as low as 970 ns before rising slowly with n_H (Fig. 4a). Now, we study P_{SS} as a function of n_H or n_C , while keeping the other quantity fixed. P_{SS} decreases rapidly as n_H increases (Fig. 4b). P_{SS} reaches its lowest value when n_C minimizes at 0.007, such that Q_2 is not excited. On the other hand, raising the cold bath's temperature impedes the reset. Increasing n_C to 0.07—exciting Q_2 more—leads P_{SS} to saturate at a higher value. Finally, consider fixing n_H and varying n_C . P_{SS} increases rapidly, then saturates near 0.36. This saturation occurs largely independently of n_H . The greater the n_H , though, the greater the initial P_{SS} .

In summary, we have demonstrated the first quantum thermal machine being deployed to accomplish a useful task. The task—reset of a superconducting qubit—is crucial to quantum information processing. The machine—a quantum absorption refrigerator formed from superconducting circuits—cools and resets the target qubit to an excited-state population lower than that achieved with state-of-the-art active reset protocols, without requiring external control. Nevertheless, the refrigeration can be turned off during the target qubit's computation cycle: One can either change the hot bath's temperature or detune a qubit out of resonance, using on-chip magnetic flux.

A salient feature of our quantum thermal machine is its use of waveguides as physical heat baths. In contrast, other experiments have emulated heat baths [50, 57]. Our

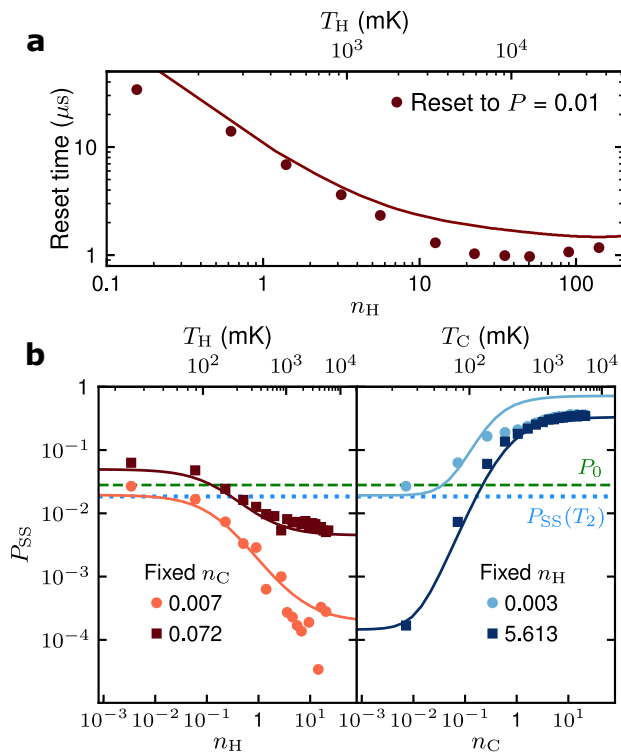


FIG. 4: Metrics of the quantum absorption refrigerator. (a) Reset time (time required for Q_3 's excited-state population to reach 0.01), as a function of the hot bath's average photon number, n_H . (b) (Left) After a 100 μ s reset protocol, Q_3 's excited state reaches a steady-state population P_{SS} . The x -axis shows n_H , translated into a temperature T_H along the top axis. Colors distinguish values of the cold bath's average photon number, n_C . (Right) P_{SS} as a function of n_C (translated into a temperature T_C on the top axis), at two n_H values. The dashed green line shows Q_3 's residual excited-state population, 0.028. The dotted blue line shows the excited-state population that Q_3 would have at the cold bath's temperature (45 mK), 0.020. All solid lines are theoretical predictions calculated from the model in Sec. II of the SI.

heat baths consist of thermal photons synthesized from quantum vacuum fluctuations and artificial microwave noise within a finite bandwidth. Our approach allows control over the baths' temperatures, the ability to tailor spectral properties of the heat baths, and the selection of the energy transitions to be heated. Thus, this method can facilitate a rigorous study of quantum thermal machines. However, our setup can be straightforwardly modified to exploit natural thermal baths, such as different-temperature plates of a dilution refrigerator. For example, superconducting coaxial cables, together with infrared-blocking filters [65], can expose the qutrits to thermal radiation emitted by hot resistors anchored to the dilution refrigerator's plates [66]. This strategy refrains from adding any significant heat load to the base temperature plate. Nor does the strategy compromise

the quantum information-processing unit's performance.

Our quantum refrigerator initiates a path toward experimental studies of quantum thermodynamics with superconducting circuits coupled to propagating thermal microwave fields. Superconducting circuits may also offer an avenue toward scaling quantum thermal machines similarly to quantum-information processors. Our experiment may inspire further development of useful, real-world applications of quantum thermodynamics to quantum information processing [67–69], thermometry [63, 66, 70], algorithmic cooling [53, 71], timekeeping [72], and entanglement generation [73]. This work marks a significant step in quantum thermodynamics toward practicality, in the spirit of how classical thermodynamics aided the industrial revolution.

ACKNOWLEDGMENTS

This work received support from the Swedish Research Council; the Knut and Alice Wallenberg Foundation through the Wallenberg Center for Quantum Technology (WACQT); the National Science Foundation, under QLCI grant OMA-2120757 and Grant No. NSF PHY-1748958; the John Templeton Foundation (award no. 62422); and NIST grant 70NANB21H055.0.

REFERENCES

- [1] E. H. Lieb and J. Yngvason, The physics and mathematics of the second law of thermodynamics, *Physics Rep.* **310**, 1 (1999).
- [2] D. Janzing, P. Wocjan, R. Zeier, R. Geiss, and Th. Beth, Thermodynamic Cost of Reliability and Low Temperatures: Tightening Landauer's Principle and the Second Law, *Int. J. Th. Phys.* **39**, 2717 (2000).
- [3] D. Egloff, O. C. O. Dahlsten, R. Renner, and V. Vedral, A measure of majorization emerging from single-shot statistical mechanics, *New Journal of Physics* **17**, 073001 (2015).
- [4] M. Horodecki and J. Oppenheim, Fundamental limitations for quantum and nanoscale thermodynamics, *Nature communications* **4**, 2059 (2013).
- [5] F. Brandão, M. Horodecki, N. Ng, J. Oppenheim, and S. Wehner, The second laws of quantum thermodynamics, *Proceedings of the National Academy of Sciences* **112**, 3275 (2015).
- [6] N. Yunger Halpern and J. M. Renes, Beyond heat baths: Generalized resource theories for small-scale thermodynamics, *Phys. Rev. E* **93**, 022126 (2016).
- [7] N. Y. Halpern, Beyond heat baths II: Framework for generalized thermodynamic resource theories, *J. Phys. A* **51**, 094001 (2018).
- [8] M. Lostaglio, D. Jennings, and T. Rudolph, Thermodynamic resource theories, non-commutativity and maximum entropy principles, *New J. Phys.* **19**, 043008 (2017).
- [9] Y. Guryanova, S. Popescu, A. J. Short, R. Silva, and P. Skrzypczyk, Thermodynamics of quantum systems with multiple conserved quantities, *Nature Comm.* **7**, 12049 (2016).

- [10] N. Yunger Halpern, P. Faist, J. Oppenheim, and A. Winter, Microcanonical and resource-theoretic derivations of the thermal state of a quantum system with noncommuting charges, *Nature Comm.* **7**, 12051 (2016).
- [11] C. Sparaciari, J. Oppenheim, and T. Fritz, Resource theory for work and heat, *Phys. Rev. A* **96**, 052112 (2017).
- [12] G. Gour, D. Jennings, F. Buscemi, R. Duan, and I. Marvian, Quantum majorization and a complete set of entropic conditions for quantum thermodynamics, *Nature communications* **9**, 5352 (2018).
- [13] Z. B. Khanian, M. N. Bera, A. Riera, M. Lewenstein, and A. Winter, Resource Theory of Heat and Work with Non-commuting Charges, *Annales Henri Poincaré* **24**, 1725 (2023).
- [14] S. W. Kim, T. Sagawa, S. De Liberato, and M. Ueda, Quantum Szilard Engine, *Phys. Rev. Lett.* **106**, 070401 (2011).
- [15] D. Gelbwaser-Klimovsky, A. Bylinskii, D. Gangloff, R. Islam, A. Aspuru-Guzik, and V. Vuletic, Single-Atom Heat Machines Enabled by Energy Quantization, *Phys. Rev. Lett.* **120**, 170601 (2018).
- [16] N. M. Myers and S. Deffner, Bosons outperform fermions: The thermodynamic advantage of symmetry, *Phys. Rev. E* **101**, 012110 (2020).
- [17] M. Lostaglio, Certifying Quantum Signatures in Thermodynamics and Metrology via Contextuality of Quantum Linear Response, *Physical Review Letters* **125**, 230603 (2020).
- [18] A. A. S. Kalaei, A. Wacker, and P. P. Potts, Violating the thermodynamic uncertainty relation in the three-level maser, *Physical Review E* **104**, L012103 (2021).
- [19] K. Hammam, H. Leitch, Y. Hassouni, and G. De Chiara, Exploiting coherence for quantum thermodynamic advantage, *New Journal of Physics* **24**, 113053 (2022).
- [20] F. C. Binder, S. Vinjanampathy, K. Modi, and J. Goold, Quantacell: Powerful charging of quantum batteries, *New Journal of Physics* **17**, 075015 (2015).
- [21] D. Jennings and T. Rudolph, Entanglement and the thermodynamic arrow of time, *Phys. Rev. E* **81**, 061130 (2010).
- [22] A. Levy and M. Lostaglio, Quasiprobability Distribution for Heat Fluctuations in the Quantum Regime, *PRX Quantum* **1**, 010309 (2020).
- [23] M. P. Woods and M. Horodecki, Autonomous Quantum Devices: When Are They Realizable without Additional Thermodynamic Costs?, *Physical Review X* **13**, 011016 (2023).
- [24] J. Roßnagel, S. T. Dawkins, K. N. Tolazzi, O. Abah, E. Lutz, F. Schmidt-Kaler, and K. Singer, A single-atom heat engine, *Science* **352**, 325 (2016).
- [25] M. T. Mitchison, M. P. Woods, J. Prior, and M. Huber, Coherence-assisted single-shot cooling by quantum absorption refrigerators, *New Journal of Physics* **17**, 115013 (2015).
- [26] K. Geerlings, Z. Leghtas, I. M. Pop, S. Shankar, L. Frunzio, R. J. Schoelkopf, M. Mirrahimi, and M. H. Devoret, Demonstrating a Driven Reset Protocol for a Superconducting Qubit, *Phys. Rev. Lett.* **110**, 120501 (2013).
- [27] X. Y. Jin, A. Kamal, A. P. Sears, T. Gudmundsen, D. Hover, J. Miloxi, R. Slattey, F. Yan, J. Yoder, T. P. Orlando, S. Gustavsson, and W. D. Oliver, Thermal and Residual Excited-State Population in a 3D Transmon Qubit, *Physical Review Letters* **114**, 240501 (2015).
- [28] P. Magnard, P. Kurpiers, B. Royer, T. Walter, J.-C. Besse, S. Gasparinetti, M. Pechal, J. Heinsoo, S. Storz, A. Blais, and A. Wallraff, Fast and Unconditional All-Microwave Reset of a Superconducting Qubit, *Phys. Rev. Lett.* **121**, 060502 (2018).
- [29] Y. Zhou, Z. Zhang, Z. Yin, S. Huai, X. Gu, X. Xu, J. Allcock, F. Liu, G. Xi, Q. Yu, H. Zhang, M. Zhang, H. Li, X. Song, Z. Wang, D. Zheng, S. An, Y. Zheng, and S. Zhang, Rapid and Unconditional Parametric Reset Protocol for Tunable Superconducting Qubits, *Nature Communications* **12**, 5924 (2021).
- [30] N. Linden, S. Popescu, and P. Skrzypczyk, How Small Can Thermal Machines Be? The Smallest Possible Refrigerator, *Physical Review Letters* **105**, 130401 (2010).
- [31] A. Levy and R. Kosloff, Quantum Absorption Refrigerator, *Physical Review Letters* **108**, 070604 (2012).
- [32] Y.-X. Chen and S.-W. Li, Quantum refrigerator driven by current noise, *EPL (Europhysics Letters)* **97**, 40003 (2012).
- [33] D. Venturelli, R. Fazio, and V. Giovannetti, Minimal Self-Contained Quantum Refrigeration Machine Based on Four Quantum Dots, *Phys. Rev. Lett.* **110**, 256801 (2013).
- [34] L. A. Correa, J. P. Palao, D. Alonso, and G. Adesso, Quantum-enhanced absorption refrigerators, *Sci. Rep.* **4**, 3949 (2014).
- [35] R. Silva, P. Skrzypczyk, and N. Brunner, Small quantum absorption refrigerator with reversed couplings, *Phys. Rev. E* **92**, 012136 (2015).
- [36] P. P. Hofer, M. Perarnau-Llobet, J. B. Brask, R. Silva, M. Huber, and N. Brunner, Autonomous quantum refrigerator in a circuit QED architecture based on a Josephson junction, *Phys. Rev. B* **94**, 235420 (2016).
- [37] A. Mu, B. K. Agarwalla, G. Schaller, and D. Segal, Qubit absorption refrigerator at strong coupling, *New Journal of Physics* **19**, 123034 (2017).
- [38] S. Nimmrichter, J. Dai, A. Roulet, and V. Scarani, Quantum and classical dynamics of a three-mode absorption refrigerator, *Quantum* **1**, 37 (2017).
- [39] J.-Y. Du and F.-L. Zhang, Nonequilibrium quantum absorption refrigerator, *New Journal of Physics* **20**, 063005 (2018).
- [40] V. Holubec and T. Novotný, Effects of noise-induced coherence on the fluctuations of current in quantum absorption refrigerators, *The Journal of Chemical Physics* **151**, 044108 (2019).
- [41] M. T. Mitchison and P. P. Potts, Physical Implementations of Quantum Absorption Refrigerators, in *Thermodynamics in the Quantum Regime: Fundamental Aspects and New Directions*, Fundamental Theories of Physics, edited by F. Binder, L. A. Correa, C. Gogolin, J. Anders, and G. Adesso (Springer International Publishing, Cham, 2018) pp. 149–174.
- [42] M. T. Mitchison, Quantum thermal absorption machines: Refrigerators, engines and clocks, *Contemporary Physics* **60**, 164 (2019).
- [43] M. T. Naseem, A. Misra, and Ö. E. Müstecaplıoğlu, Two-body quantum absorption refrigerators with optomechanical-like interactions, *Quantum Science and Technology* **5**, 035006 (2020).
- [44] S. K. Manikandan, É. Jussiau, and A. N. Jordan, Autonomous quantum absorption refrigerators, *Physical Review B* **102**, 235427 (2020).
- [45] P. Arrangoiz-Arriola, E. A. Wollack, M. Pechal, J. D.

- Witmer, J. T. Hill, and A. H. Safavi-Naeini, Coupling a Superconducting Quantum Circuit to a Phononic Crystal Defect Cavity, *Phys. Rev. X* **8**, 031007 (2018).
- [46] B. Bhandari and A. N. Jordan, Minimal two-body quantum absorption refrigerator, *Phys. Rev. B* **104**, 075442 (2021).
- [47] M. Kloc, K. Meier, K. Hadjikyriakos, and G. Schaller, Superradiant Many-Qubit Absorption Refrigerator, *Phys. Rev. Applied* **16**, 044061 (2021).
- [48] M. W. AlMasri and M. R. B. Wahiddin, Bargmann Representation of Quantum Absorption Refrigerators, *Reports on Mathematical Physics* **89**, 185 (2022).
- [49] H. Okane, S. Kamimura, S. Kukita, Y. Kondo, and Y. Matsuzaki, *Quantum Thermodynamics applied for Quantum Refrigerators cooling down a qubit* (2022).
- [50] G. Maslennikov, S. Ding, R. Hablützel, J. Gan, A. Roulet, S. Nimmrichter, J. Dai, V. Scarani, and D. Matsukevich, Quantum absorption refrigerator with trapped ions, *Nature Communications* **10**, 202 (2019).
- [51] S. K. Manikandan and S. Qvarfort, Optimal quantum parametric feedback cooling, *Physical Review A* **107**, 023516 (2023).
- [52] T. Karmakar, É. Jussiau, S. K. Manikandan, and A. N. Jordan, Cyclic Superconducting Quantum Refrigerators Using Guided Fluxon Propagation, arXiv:2212.00277 10.48550/arxiv.2212.00277 (2022).
- [53] J. Baugh, O. Moussa, C. A. Ryan, A. Nayak, and R. Laflamme, Experimental implementation of heat-bath algorithmic cooling using solid-state nuclear magnetic resonance, *Nature* **438**, 470 (2005).
- [54] A. Solfanelli, A. Santini, and M. Campisi, Quantum thermodynamic methods to purify a qubit on a quantum processing unit, *AVS Quantum Science* **4**, 026802 (2022).
- [55] L. Buffoni and M. Campisi, Cooperative quantum information erasure, *Quantum* **7**, 961 (2023).
- [56] A. Ronzani, B. Karimi, J. Senior, Y. Chang, J. T. Peltonen, C. Chen, and J. P. Pekola, Tunable photonic heat transport in a quantum heat valve, *Nature Physics* **14**, 991 (2018).
- [57] J. Klatzow, J. N. Becker, P. M. Ledingham, C. Weinzel, K. T. Kaczmarek, D. J. Saunders, J. Nunn, I. A. Walmsley, R. Uzdin, and E. Poem, Experimental Demonstration of Quantum Effects in the Operation of Microscopic Heat Engines, *Phys. Rev. Lett.* **122**, 110601 (2019).
- [58] K. Y. Tan, M. Partanen, R. E. Lake, J. Govenius, S. Masuda, and M. Möttönen, Quantum-circuit refrigerator, *Nature Communications* **8**, 15189 (2017).
- [59] W. Ren, W. Liu, C. Song, H. Li, Q. Guo, Z. Wang, D. Zheng, G. S. Agarwal, M. O. Scully, S.-Y. Zhu, H. Wang, and D.-W. Wang, Simultaneous Excitation of Two Noninteracting Atoms with Time-Frequency Correlated Photon Pairs in a Superconducting Circuit, *Physical Review Letters* **125**, 133601 (2020).
- [60] J. Koch, T. M. Yu, J. Gambetta, A. A. Houck, D. I. Schuster, J. Majer, A. Blais, M. H. Devoret, S. M. Girvin, and R. J. Schoelkopf, Charge-insensitive qubit design derived from the Cooper pair box, *Phys. Rev. A* **76**, 042319 (2007).
- [61] M. D. Reed, B. R. Johnson, A. A. Houck, L. DiCarlo, J. M. Chow, D. I. Schuster, L. Frunzio, and R. J. Schoelkopf, Fast reset and suppressing spontaneous emission of a superconducting qubit, *Applied Physics Letters* **96**, 203110 (2010).
- [62] J. M. Fink, L. Steffen, P. Studer, L. S. Bishop, M. Baur, R. Bianchetti, D. Bozyigit, C. Lang, S. Filipp, P. J. Leek, and A. Wallraff, Quantum-To-Classical Transition in Cavity Quantum Electrodynamics, *Phys. Rev. Lett.* **105**, 163601 (2010).
- [63] M. Scigliuzzo, A. Bengtsson, J.-C. Besse, A. Wallraff, P. Delsing, and S. Gasparinetti, Primary Thermometry of Propagating Microwaves in the Quantum Regime, *Physical Review X* **10**, 041054 (2020).
- [64] Module 10: Absorption refrigeration, CIBSE Journal (2009), <https://www.cibsejournal.com/cpd/modules/2009-11/>.
- [65] R. Rehammar and S. Gasparinetti, Low-Pass Filter With Ultrawide Stopband for Quantum Computing Applications, *IEEE Transactions on Microwave Theory and Techniques* doi: 10.1109/TMTT.2023.3238543, 10.1109/TMTT.2023.3238543 (2023).
- [66] Z. Wang, M. Xu, X. Han, W. Fu, S. Puri, S. M. Girvin, H. X. Tang, S. Shankar, and M. H. Devoret, Quantum Microwave Radiometry with a Superconducting Qubit, *Physical Review Letters* **126**, 180501 (2021).
- [67] M. Fellous-Asiani, J. H. Chai, R. S. Whitney, A. Auffèves, and H. K. Ng, Limitations in Quantum Computing from Resource Constraints, *PRX Quantum* **2**, 040335 (2021).
- [68] A. Auffèves, Quantum Technologies Need a Quantum Energy Initiative, *PRX Quantum* **3**, 020101 (2022).
- [69] M. Aifer and S. Deffner, From quantum speed limits to energy-efficient quantum gates, *New Journal of Physics* **24**, 055002 (2022).
- [70] M. Mehboudi, A. Sanpera, and L. A. Correa, Thermometry in the quantum regime: Recent theoretical progress, *Journal of Physics A: Mathematical and Theoretical* **52**, 303001 (2019).
- [71] Á. M. Alhambra, M. Lostaglio, and C. Perry, Heat-Bath Algorithmic Cooling with optimal thermalization strategies, *Quantum* **3**, 188 (2019).
- [72] P. Erker, M. T. Mitchison, R. Silva, M. P. Woods, N. Brunner, and M. Huber, Autonomous Quantum Clocks: Does Thermodynamics Limit Our Ability to Measure Time?, *Physical Review X* **7**, 031022 (2017).
- [73] J. B. Brask, G. Haack, N. Brunner, and M. Huber, Autonomous quantum thermal machine for generating steady-state entanglement, *New Journal of Physics* **17**, 113029 (2015).
- [74] S. E. Nigg, H. Paik, B. Vlastakis, G. Kirchmair, S. Shankar, L. Frunzio, M. H. Devoret, R. J. Schoelkopf, and S. M. Girvin, Black-Box Superconducting Circuit Quantization, *Phys. Rev. Lett.* **108**, 240502 (2012).
- [75] H. J. Carmichael and D. F. Walls, Master equation for strongly interacting systems, *Journal of Physics A: Mathematical, Nuclear and General* **6**, 1552 (1973).

SUPPLEMENTARY INFORMATION

1. Full experimental setup and parameters

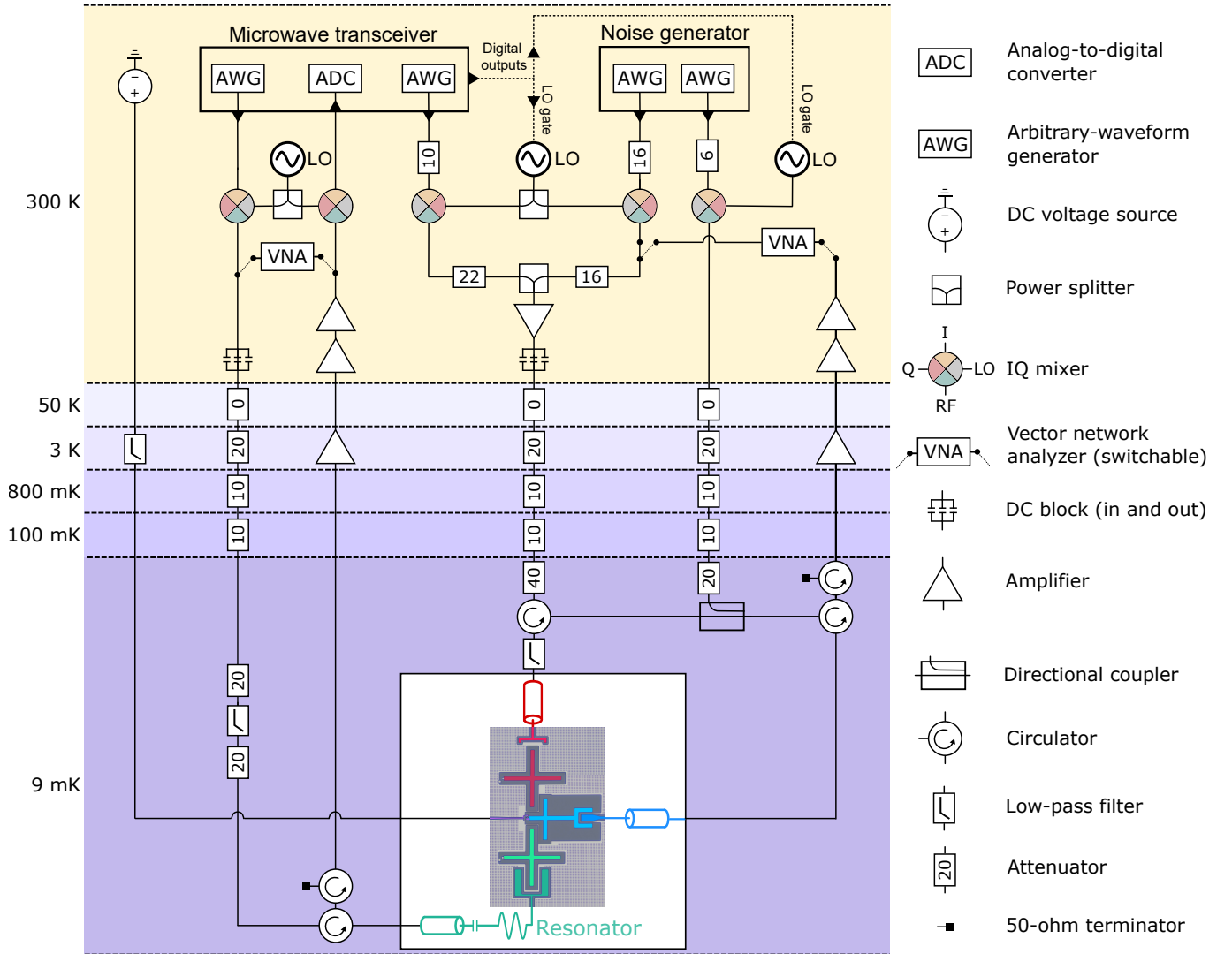


FIG. S1: Complete experimental set-up. See text for description. The in-phase-quadrature (IQ) mixers' ports I and Q are both used to connect to the microwave transceiver. However, only port I is shown to be wired; port Q is omitted for clarity. Digital outputs from the microwave transceiver are used to gate the local oscillators (LO) to produce pulses of thermal microwave modes.

Figure S1 shows a schematic of the experimental set-up used to study our quantum absorption refrigerator (QAR). The QAR is packaged in a copper enclosure and mounted on the mixing-chamber stage of a dilution refrigerator that reaches 9 mK. The QAR is packaged in multiple layers: two nested copper enclosures shield the QAR from electromagnetic waves. A μ -metal enclosure protects the QAR from low-frequency magnetic fields. Microwave fields (both coherent and thermal) are routed to the QAR through highly attenuated input coaxial lines. The outgoing fields are routed through the output lines and are boosted by a cryogenic high electron-mobility transistor (HEMT) amplifier (provided by Low Noise Factory) at 3 K and by room-temperature amplifiers. Microwave circulators separate the input and output signals. The resonator, dispersively coupled to qubit Q_3 , is probed by a microwave feedline in reflection mode. We probe and drive Q_1 and Q_2 , via the waveguide coupled to each, using two attenuated coaxial lines. Taking advantage of the non-overlapping frequencies of the relevant transitions, the outgoing fields from the hot and the cold waveguide are combined with the aid of a directional coupler and forwarded to the same output line.

We use a microwave transceiver (Vivace from Intermodulation Products, Sweden), with in-phase-quadrature (IQ)

Parameter	Symbol	Value
Q_1 mode frequency	$\omega_1/(2\pi)$	5.327 GHz
Q_2 mode-tunable frequency range	$\omega_2/(2\pi)$	4.2 GHz to 4.9 GHz
Q_2 resonant frequency	$\omega_2^{\text{res}}/(2\pi)$	4.629 GHz
Q_3 mode frequency	$\omega_3/(2\pi)$	3.725 GHz
Q_1 anharmonicity	$\alpha_1/(2\pi)$	-213.4 MHz
Q_2 anharmonicity	$\alpha_2/(2\pi)$	-205.1 MHz
Q_3 anharmonicity	$\alpha_3/(2\pi)$	-237.8 MHz
Q_1 radiative-emission rate	$\Gamma_1/(2\pi)$	70 kHz
Q_2 radiative-emission rate	$\Gamma_2/(2\pi)$	7.2 MHz
Q_3 energy-relaxation time	T_{relax}	16.8 μs
Three-body-coupling rate	$A/(2\pi)$	3.2 MHz

TABLE S1: Experimentally measured parameters' values.

mixers and local oscillators (LO), for driving the qudits and for readout measurements of Q_3 . The physical connections can be switched to a vector network analyzer (VNA). The VNA is used for continuous-wave spectroscopy that allows for basic characterization, e.g., of a qudit's frequency and anharmonicity.

The waveguide coupled to Q_1 is populated with synthesized thermal microwave modes limited to a 50 MHz bandwidth centered at the qubit's frequency. An analogous statement concerns the waveguide coupled to Q_2 . To populate the waveguides, we first continuously generate voltage noise with a white (flat) spectral density, using an arbitrary-waveform generator (AWG) limited to a 50 MHz bandwidth centered at a frequency of 100 MHz. The equipment used is a Keysight 3202A, which is limited to a 500 MHz bandwidth. Next, the generated noise is up-converted with IQ mixers and microwave tones (≈ 4 GHz to 6 GHz) generated by an LO. Finally, the resulting continuous thermal radiation is chopped into pulses synchronized with Q_3 -state readouts (see Fig. 3 in the main text). This process was performed via modulation (gating) of the LO outputs (Anapico APMS20G-4-ULN), with help from the transceiver's digital logic outputs, over time intervals of 10 ns and longer. To characterize the qudits (e.g., to determine their frequencies), we can switch the input/output lines to VNA. Furthermore, to observe the three-body interactions with coherent drives (see Fig. 2 in the main text), we can switch qubit Q_1 's input line to the transceiver's AWG. (Certain equipment, instruments, software, or materials are identified in this paper in order to specify the experimental procedure adequately. Such identification is not intended to imply recommendation or endorsement of any product or service by NIST, nor is it intended to imply that the materials or equipment identified are necessarily the best available for the purpose.)

Table S1 shows the QAR's experimentally inferred parameters.

2. Theoretical model

The Hamiltonian of our QAR's three-qudit system can be written as

$$H = \sum_{i=1}^3 \left(\tilde{\omega}_i \hat{a}_i^\dagger \hat{a}_i + \alpha_i \hat{a}_i^\dagger \hat{a}_i^\dagger \hat{a}_i \hat{a}_i / 2 \right) + g_{12} \left(\hat{a}_1^\dagger \hat{a}_2 + \hat{a}_1 \hat{a}_2^\dagger \right) + g_{23} \left(\hat{a}_2^\dagger \hat{a}_3 + \hat{a}_2 \hat{a}_3^\dagger \right). \quad (\text{S1})$$

\hat{a}_i and \hat{a}_i^\dagger denote qudit Q_i 's annihilation and creation operators. $\tilde{\omega}_i$ and α_i denote qudit Q_i 's bare mode frequency and anharmonicity. g_{12} (g_{23}) denotes the rate of the coupling between qudits Q_1 and Q_2 (qudits Q_2 and Q_3).

We engineer an effective three-body interaction by meeting the resonance condition $\omega_1 + \omega_3 = 2\omega_2 + \alpha_2$ and using Josephson junctions that facilitate the four-wave mixing [59]. The three-body interaction interchanges the three-qudit states $|101\rangle$ and $|020\rangle$ (see the notation and Fig. 1c in the main text).

We now introduce an approximation to H . Denote by A the rate at which $|101\rangle$ and $|020\rangle$ couple coherently. H is well-approximated by the effective Hamiltonian

$$H_{\text{eff}} = \sum_{i=1}^3 \omega_i \hat{a}_i^\dagger \hat{a}_i + \sum_{i,j=1}^3 \frac{\alpha_{ij}}{2} \hat{a}_i^\dagger \hat{a}_i \hat{a}_j^\dagger \hat{a}_j + A (|101\rangle\langle 020| + |020\rangle\langle 101|). \quad (\text{S2})$$

The simplification follows from black-box quantization [74] and second-order time-independent perturbation theory [59]. H_{eff} depends on dressed modes associated with annihilation and creation operators \hat{a}_i and \hat{a}_i^\dagger , dressed-mode

frequencies ω_i , and self and cross-Kerr coupling rates α_{ij} .

Let us introduce into the model a drive as shown in Fig. 2 of the main text. This coherent drive is applied to Q_1 at the drive frequency ω_d and the rate Ω . Upon adding a drive term to H_{eff} , we apply the rotating-wave approximation. We obtain the full Hamiltonian

$$H_{D1} = \sum_{i=1}^3 \delta_i \hat{a}_i^\dagger \hat{a}_i + \sum_{i,j=1}^3 \frac{\alpha_{ij}}{2} \hat{a}_i^\dagger \hat{a}_i \hat{a}_j^\dagger \hat{a}_j + A (|101\rangle\langle 020| + |020\rangle\langle 101|) + \frac{\Omega}{2} (\hat{a}_1 + \hat{a}_1^\dagger). \quad (\text{S3})$$

The effective frequency $\delta_i = \omega_d - \omega_i$.

To model the measurements of Fig. 2, we solve a Lindblad quantum master equation:

$$\frac{\partial \rho}{\partial t} = -\frac{i}{\hbar} [H_{D1}, \rho] + \sum_{i=1}^3 \Gamma_i \mathcal{D}[\hat{a}_i, \rho]. \quad (\text{S4})$$

We model the waveguides as zero-temperature baths (with average occupation numbers of 0). The qudits can interact with such baths just through spontaneous emission [75]. We have suppressed the time dependence of ρ in our notation. $\Gamma_{i=1,2}$ denotes the rate at which qudit Q_i couples to its waveguide. Γ_3 , Q_3 's natural energy-relaxation rate, is related to the qubit's energy-relaxation time T_{relax} through $\Gamma_3 = 1/T_{\text{relax}}$. The dissipator superoperator \mathcal{D} is defined through

$$\mathcal{D}[A, B] = ABA^\dagger - \frac{1}{2} (A^\dagger AB + BA^\dagger A), \quad (\text{S5})$$

for operators A and B .

To model the QAR interacting with two heat baths, we limit our analysis to a subspace of the full Hilbert space. This subspace is spanned by the basis $\mathcal{B} = \{|000\rangle, |100\rangle, |010\rangle, |001\rangle, |020\rangle, |101\rangle\}$. The population of $|i\rangle \in \mathcal{B}$ is $p_i := \rho_{ii} := \langle i | \rho | i \rangle$. We formulate a rate equation for these populations. To capture the coherent exchanges between $|101\rangle$ and $|020\rangle$, we also include an off-diagonal element $\rho_{\text{coh}} = \langle 101 | \rho | 020 \rangle$ in the model. Combining these ingredients, we introduce the rate equation for the populations:

$$\frac{d}{dt} \begin{pmatrix} p_{|000\rangle}(t) \\ p_{|100\rangle}(t) \\ p_{|010\rangle}(t) \\ p_{|001\rangle}(t) \\ p_{|020\rangle}(t) \\ p_{|101\rangle}(t) \\ \rho_{\text{coh}}(t) \end{pmatrix} = R_P \begin{pmatrix} p_{|000\rangle}(t) \\ p_{|100\rangle}(t) \\ p_{|010\rangle}(t) \\ p_{|001\rangle}(t) \\ p_{|020\rangle}(t) \\ p_{|101\rangle}(t) \\ \rho_{\text{coh}}(t) \end{pmatrix}. \quad (\text{S6})$$

The rate matrix R_P is defined as

$$R_P := \begin{pmatrix} -\Gamma_{1\uparrow} + \Gamma_{2\uparrow} + \Gamma_{3\uparrow} & \Gamma_{1\downarrow} & \Gamma_{2\downarrow} & \Gamma_{3\downarrow} & 0 & 0 & 0 \\ \Gamma_{1\uparrow} & -(\Gamma_{1\downarrow} + \Gamma_{3\uparrow}) & 0 & 0 & 0 & \Gamma_{3\downarrow} & 0 \\ \Gamma_{2\uparrow} & 0 & -(\Gamma_{2\downarrow} + 2\Gamma_{2\uparrow}) & 0 & 2\Gamma_{2\downarrow} & 0 & 0 \\ \Gamma_{3\uparrow} & 0 & 0 & -(\Gamma_{3\downarrow} + \Gamma_{1\uparrow}) & 0 & \Gamma_{1\downarrow} & 0 \\ 0 & 0 & 2\Gamma_{2\uparrow} & 0 & -2\Gamma_{2\downarrow} & 0 & 2A \\ 0 & \Gamma_{3\uparrow} & 0 & \Gamma_{1\uparrow} & 0 & -(\Gamma_{1\downarrow} + \Gamma_{3\downarrow}) & -2A \\ 0 & 0 & 0 & 0 & -A & A & \Gamma_C \end{pmatrix} \quad (\text{S7})$$

We define the Γ 's as follows. Denote by n_i the average number of synthesized thermal photons in the waveguide coupled to qudit Q_i ; by $n_{i,\text{res}}$, the average number of native thermal (residual) photons already present in waveguide $i = 1, 2$; and by $n_{3,\text{res}}$, the effective average number of thermal photons in qudit Q_3 's environment. In terms of these quantities, we define lowering rates $\Gamma_{i\downarrow} = \Gamma_i(n_i + n_{i,\text{res}} + 1)$ and raising rates $\Gamma_{i\uparrow} = \Gamma_i(n_i + n_{i,\text{res}})$ for the qudits $i = \{1, 2\}$, as well as $\Gamma_{3\downarrow} = \Gamma_3(n_{3,\text{res}} + 1)$ and $\Gamma_{3\uparrow} = \Gamma_3 n_{3,\text{res}}$. For brevity, Eq. (S7) also contains $\Gamma_C = (-2\Gamma_{2\downarrow} + 2\Gamma_{2\uparrow} + \Gamma_{1\downarrow} + \Gamma_{1\uparrow} + \Gamma_{3\downarrow} + \Gamma_{3\uparrow})/4$.

To model the data in Figs. 3b and 4b, we solve Eq. (S6) with the initial condition

$$(p_{|000\rangle}(0), p_{|100\rangle}(0), p_{|010\rangle}(0), p_{|001\rangle}(0), p_{|020\rangle}(0), p_{|101\rangle}(0), \rho_{\text{coh}}(0)) = (0, 0, 0, 1, 0, 0, 0).$$

This vector represents the initial state $|001\rangle$.

Having introduced our dynamical model, we review the coefficient of performance (COP), following Ref. [36]. Denote by \dot{Q}_3 the current of heat drawn from the target system. Denote by \dot{Q}_1 the current of heat drawn by qubit 1 from the hot bath. An absorption refrigerator's COP equals the ratio of one to the other:

$$\text{COP} := \dot{Q}_3 / \dot{Q}_1. \quad (\text{S8})$$

We calculate the COP at the refrigerator's steady state. The steady-state heat current drawn from bath $i \in \{1, 2, 3\}$ is

$$\dot{Q}_i = \text{Tr}(H \mathcal{L}_i \rho(\infty)). \quad (\text{S9})$$

The Lindbladian therein acts as $\mathcal{L}_i \rho = \Gamma_i \left\{ (n_i + n_{i,\text{res}} + 1) \mathcal{D}[\tilde{a}_i, \rho] + (n_i + n_{i,\text{res}}) \mathcal{D}[\tilde{a}_i^\dagger, \rho] \right\}$.

3. Rabi population-measurement scheme

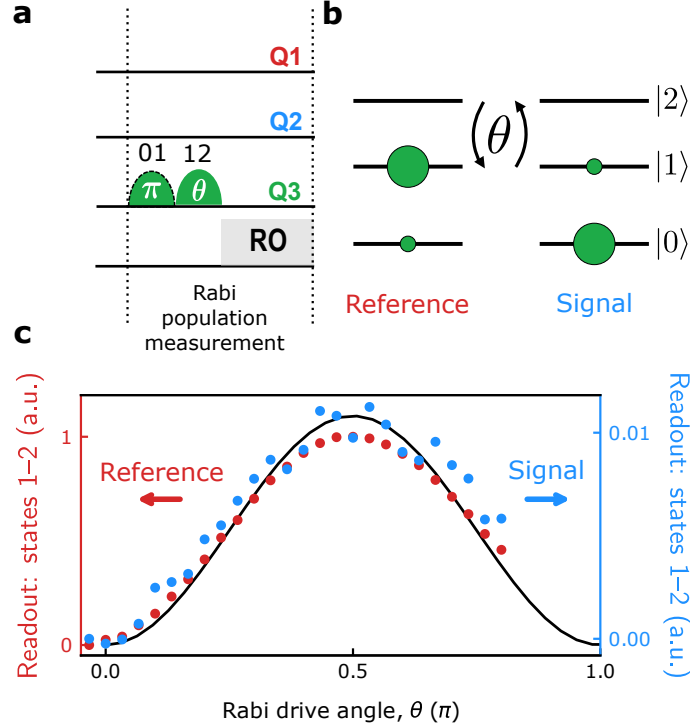


FIG. S2: Rabi measurement of the population in qubit Q_3 's $|1\rangle$ level. (a) Pulse sequence for the scheme. The notation 0–1 (1–2) indicates that the pulse drives the transition $|0\rangle \leftrightarrow |1\rangle$ ($|1\rangle \leftrightarrow |2\rangle$). θ denotes the pulse drive's Rabi angle. The pulse with the dashed outline is present in the reference measurement and absent from the signal measurement. The readout (RO) is performed in the subspace $\text{span}\{|1\rangle, |2\rangle\}$. (b) Representation of the relative distribution of populations across $|0\rangle$, $|1\rangle$, and $|2\rangle$. (c) Rabi oscillations. The Rabi oscillation resulting from the 1–2 pulse provides a reference trace (red). The Rabi oscillation produced without the 1–2 pulse provides the signal—the actual population trace (blue).

Figure S2 shows the pulse sequence for measuring Q_3 's level- $|1\rangle$ population more accurately than standard qubit readout allows [26, 27]. This Rabi scheme involves the Q_3 energy levels $|0\rangle$, $|1\rangle$, and $|2\rangle$. (We measure the qubit-state readout in the subspace $\text{span}\{|1\rangle, |2\rangle\}$.) The scheme involves also two different Rabi oscillations. We drive Rabi oscillations between $|1\rangle$ and $|2\rangle$ in each of two cases: with and without a prior π pulse in the subspace $\text{span}\{|0\rangle, |1\rangle\}$. The prior pulse interchanges the populations of $|0\rangle$ and $|1\rangle$ [see the 0–1 pulse with the dashed outline in Fig. S2(a)]. We denote these Rabi oscillations' amplitudes by r and s , respectively. The population of Q_3 's $|1\rangle$ state is $s/(r + s)$. This method works if $|2\rangle$ is empty and so can serve as a reference for zero population.

4. Refrigeration's dependence on cold-bath temperature

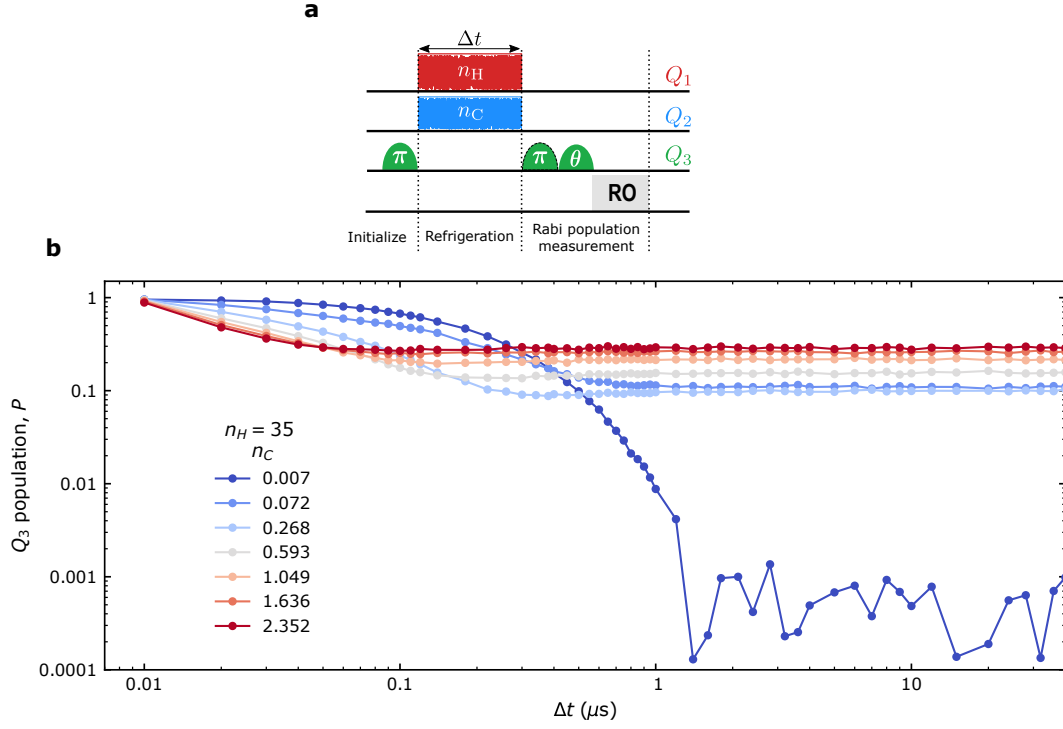


FIG. S3: Refrigeration's dependence on cold-bath temperature. (a) Pulse scheme. (b) Population of qubit Q_3 's $|1\rangle$ level, as a function of the time duration Δt of the thermal-microwave-mode pulses, at select values of the average number n_C of thermal photons in the cold bath. The average number n_H of thermal photons in the hot bath is fixed at the high value 35.

Figure S3 shows the population of Q_3 's $|1\rangle$ state, P . We depict P as a function of the duration Δt for which the thermal microwave modes are applied. We present these data at several values of the average number n_C of photons in the cold bath. The average number n_H of hot-bath thermal photons is a high value, 35.

Increasing n_C populates Q_2 's excited states incoherently, rendering the qutrit's state mixed [63]. The mixing hinders the three-body process $|101\rangle \rightarrow |020\rangle$. The refrigeration is impeded, and so the steady-state P increases.

5. Refrigeration of Q_3 initiated in its natural steady state

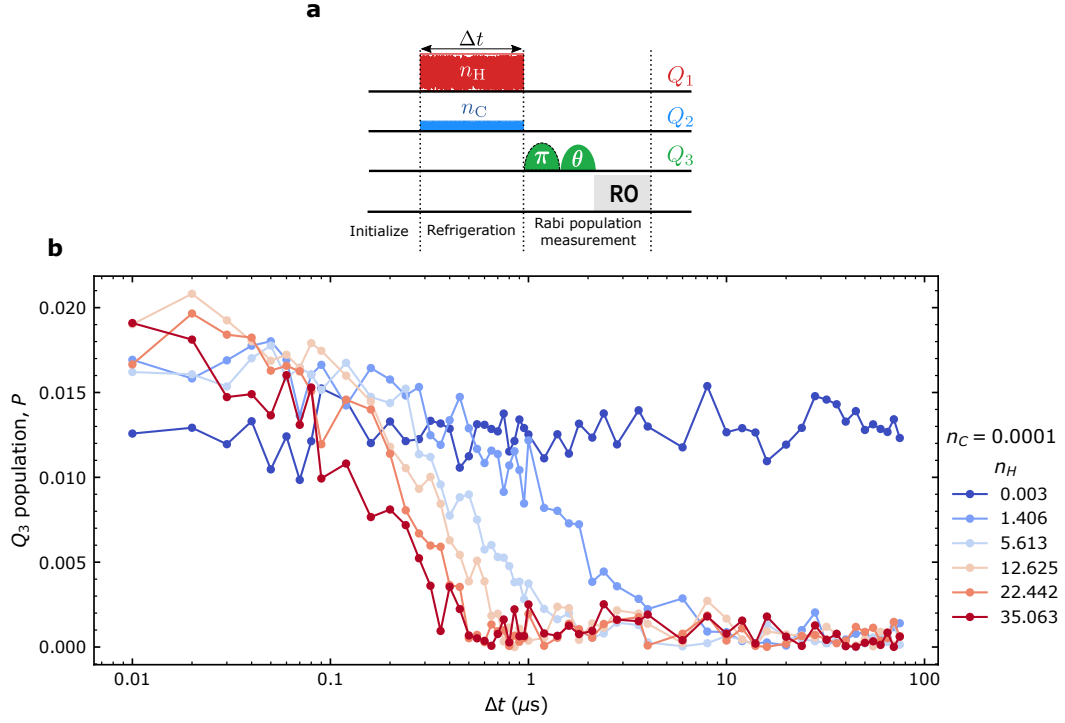


FIG. S4: Refrigeration of target qubit initialized with a residual $|1\rangle$ population of 0.020. (a) Pulse scheme. The qubit is not initialized entirely in the excited state. (b) Q_3 's excited-state population, P , as a function of the time duration Δt of the thermal-microwave-mode pulses, for select values of the average number n_H of thermal photons in the hot bath.

In this study, we begin with Q_3 in the steady state that results from Q_3 's equilibrating as much as possible with its environment (the state may, in fact, be far from equilibrium). According to our measurements, Q_3 's $|1\rangle$ level has a population P of 0.028 in this state. We allow our refrigerator to run for a duration Δt , then perform Rabi population measurement of $|1\rangle$. (See the pulse scheme in Fig. S4a.) P is plotted as a function of Δt in Fig. S4. Here, P begins at a much less value than in the main text's Fig. 3b. Therefore, P reaches its long-time value, here, by an earlier time ≈ 500 ns.